Performance of MIMO Schemes with Partial Channel Knowledge

S. Shilo, A. J. Weiss, *Fellow, IEEE,* and A. Averbuch

Abstract

Multiple antenna techniques are used to enhance wireless links and therefore have been studied extensively. Many practical systems differ from the ideal schemes discussed in the literature. One example is the lack of precise channel information at the transmitter. We evaluate analytically the performance of several multiple input multiple output (MIMO) techniques that use partial channel knowledge. Specifically, we analyze schemes which are used in Worldwide Inter-operability for Microwave Access (WiMAX) and are also supported by Long Term Evolution (LTE) systems. All the results are supported by simulations.

Index Terms

MIMO systems, Partial Channel Knowledge, WiMAX, LTE.

I. Introduction

Multiple input multiple output (MIMO) techniques have been incorporated in all specifications of the recently developed wireless communications systems, including Long Term Evolution (LTE) and Worldwide Inter-operability for Microwave Access (WiMAX) technologies. MIMO schemes include Alamouti's space-time coding [1], spatial multiplexing and a few transmit beamforming methods.

Multiple antennas are employed on both sides of the communications channel in most MIMO systems. In time division duplex (TDD) the same frequency is used by both sides and the same

S. Shilo and A. J. Weiss are with the School of Electrical Engineering, Tel Aviv University.

A. Averbuch is with the School of Computer Science, Tel Aviv University.

Manuscript received ???, 2009.

antennas are used for transmission and reception. Thus, the channel matrix can be estimated by each side based on the reception of a known waveform. However, due to cost considerations, early generations of WiMAX and LTE restrict the mobile station (MS) to one transmit antenna although two or more antennas are used for reception. Thus, the transmission from the MS can be used to estimate the channel between one of the MS antennas and all the base station (BS) antennas. The channel between the BS antennas and the other receive antennas of the MS is not known to the BS. As a result, transmit beamforming schemes employed by the BS, are limited to partial channel knowledge. This problem can be solved by allowing the MS to report its channel estimates to the BS [2]. However, this closed loop scheme requires a rather complex receiver at the MS.

Communications using partial state information has been thoroughly analyzed in the literature. The performance of various scalar and vector quantizers has been discussed in [3]. It is shown that a few feedback bits provide performance which is similar to that of beamforming with perfect channel knowledge. Limited feedback and quantized codebook are discussed in [4]. It is shown that the desired codebooks depend on the number of transmit antennas (but not on the number of receive antennas) and on the number of code words. It is also shown that a sufficient condition for full diversity is a codebook cardinality not less than the number of transmit antennas. The relation between the signal to noise ratio (SNR) and the amount of the required feedback, for the case of MIMO broadcast channels, is analyzed in [5]. It is shown that for zero forcing precoding to achieve full multiplexing gain, the required number of feedback bits per user increases linearly with the SNR. As the SNR increases, multi-user interference becomes more dominant and more feedback bits are required to achieve the multiplexing gain. More analysis of feedback methods and their impact have been thoroughly studied in [6], [7].

The partial knowledge, discussed in this paper, is different from the partial state information considered so far. We assume here that only part of the channel matrix is perfectly known while the other part is unknown. Our goal is to analyze practical transmission schemes using partial channel knowledge.

In Section II, we describe two transmission schemes. In the first scheme the same waveform is transmitted by all the antennas. The second scheme discusses spatial multiplexing where one waveform is transmitted by one antenna pair and a different waveform is transmitted by a different antenna pair. We evaluate the symbol error probability, the diversity order and the array

gain for each scheme. Simulation results are presented in Section III.

II. Analysis of Transmission Schemes Using partial channel knowledge

Assume a BS equipped with 4 antennas and a MS with only 2 antennas. One of the MS antennas is used for transmission while both antennas are used for reception. This mode is typical in the initial versions of the 4G networks such as LTE and WiMAX [8], [9]. Let us denote the channel between the i-th MS antenna and the j-th BS antenna by h_{ij} where $i \in \{0,1\}$; $j \in \{0,1,2,3\}$. See Figure A.1.

The MS transmits a known sequence (sometimes called Uplink Sounding), which will be used at the BS to estimate the channel, assuming channel reciprocity. This pertains mostly to TDD systems. Since only one antenna is used in the MS for transmission, the sounding signal will be transmitted from one antenna only. Assume that the channel estimation at the BS is perfect and then channels h_{00}, h_{01}, h_{02}, h_{03} are known and the channels h_{10}, h_{11}, h_{12}, h_{13} are unknown.

There are several transmission schemes that can be used by the BS. The question is which scheme is the most beneficial. We compare two schemes.

1) Single stream transmission using maximal ratio transmission (MRT) beamforming with all 4 antennas at the BS and maximal ratio combining (MRC) at the MS receiver. Beamforming is performed towards the single transmitting MS antenna. This scheme is denoted hereinafter by 4×2 MRT;
2) Two different streams transmission. Each steam is transmitted from a different antenna pair at the BS. Each pair is using MRT beamforming. This is a type of spatial multiplexing (SM) and therefore the scheme is denoted hereinafter by SM-MRT.

Since there is a single stream in the first scheme and two streams in the second, the same total bit rate will be used for a fair comparison between the schemes. The same approach is used for comparing Alamouti's space-time coding with spatial multiplexing. See for example [10], [11].

A. 4×2 MRT

In this scheme, Uplink (UL) Sounding is performed from only one MS antenna. The BS is able to estimate $\boldsymbol{h}_0^* = [h_{00}, h_{01}, h_{02}, h_{03}]$ whereas $\boldsymbol{h}_1^* = [h_{10}, h_{11}, h_{12}, h_{13}]$ is unknown. We use $[\cdot]^*$ to denote conjugate transpose. Since only the channel $\boldsymbol{h}_0$ is known, the transmitter uses only this partial information for beamforming towards the first antenna. The analysis in the sequel is

done under the assumptions that the different channels experience independent Rayleigh fading and quadrature phase shift keying (QPSK) modulation is used by the BS. Using $\boldsymbol{w} = \boldsymbol{h}_0/\|\boldsymbol{h}_0\|$ as the beamforming weighting, the transmitted 4×1 vector is $\boldsymbol{w}s$ and the received vector at the two receiver antennas is given by

$$\begin{bmatrix} r_0 \\ r_1 \end{bmatrix} = \begin{bmatrix} \boldsymbol{h}_0^* \\ \boldsymbol{h}_1^* \end{bmatrix} \boldsymbol{w}s + \rho\,\boldsymbol{n} = \begin{bmatrix} \boldsymbol{h}_0^* \\ \boldsymbol{h}_1^* \end{bmatrix} \frac{\boldsymbol{h}_0}{\|\boldsymbol{h}_0\|} s + \rho\,\boldsymbol{n} = \boldsymbol{a}s + \rho\boldsymbol{n}. \tag{II.1}$$

Here s is the baseband QPSK signal, $\boldsymbol{n}$ is a zero mean, Gaussian vector with covariance equal to the 2×2 identity matrix, and ρ^2 is the noise variance. The vector $\boldsymbol{a}$ represent the effect of the beamforming and the channel on the signal and its entries can be deduced from the above equation. Assuming that the MS knows the channel and therefore $\boldsymbol{a}$ one can left multiply the above equation by the pseudo inverse of $\boldsymbol{a}$. This processing is known as MRC and the result is

$$\hat{s} = s + \rho \left(\|\boldsymbol{h}_0\|^2 + |\boldsymbol{h}_1^* \boldsymbol{h}_0|^2 \|\boldsymbol{h}_0\|^{-2} \right)^{-1} \left[\begin{array}{cc} \|\boldsymbol{h}_0\| \ , & \boldsymbol{h}_1^* \boldsymbol{h}_0 \|\boldsymbol{h}_0\|^{-1} \end{array} \right] \boldsymbol{n}. \tag{II.2}$$

The post processing SNR is then given by

$$\gamma = \rho^{-2}(\|\boldsymbol{h}_0\|^2 + |\boldsymbol{h}_1^* \boldsymbol{h}_0|^2 \|\boldsymbol{h}_0\|^{-2}). \tag{II.3}$$

The error probability, given the channel matrix $\boldsymbol{H} = [\boldsymbol{h}_0, \boldsymbol{h}_1]^*$, is

$$\Pr\{\text{error}|\boldsymbol{H}\} = 2Q\left(\sqrt{\gamma}\right) - Q^2\left(\sqrt{\gamma}\right) \approx \frac{1}{6}\exp\left(-\gamma/2\right) + \frac{1}{2}\exp\left(-2\gamma/3\right). \tag{II.4}$$

We used the approximation given in [12] for the Q-Function. Note that $|\boldsymbol{h}_1 \boldsymbol{h}_0{}^*|^2 \|\boldsymbol{h}_0\|^{-2}$ can be rewritten as

$$|\boldsymbol{h}_1{}^* \boldsymbol{h}_0|^2 \|\boldsymbol{h}_0\|^{-2} = \|\boldsymbol{h}_1\|^2 \cos^2(\alpha) = \cos^2(\alpha) \sum_{i=0}^{3} |h_{1i}|^2, \tag{II.5}$$

where α, which is the angle between the vectors $\boldsymbol{h}_0$ and $\boldsymbol{h}_1$, is defined by $\cos\alpha = |\boldsymbol{h}_1^* \boldsymbol{h}_0|(\|\boldsymbol{h}_0\|\,\|\boldsymbol{h}_1\|)^{-1}$. Substituting Eq. II.5 into Eq. II.4 and denoting $\xi_i = |h_{0i}|$ and $\psi_i = |h_{1i}|$, then the error probability for any given α is

$$\begin{aligned} \Pr\{\text{error}|\alpha\} \approx & \int_0^\infty \cdots \int_0^\infty \left[\frac{1}{6}\exp\left(-\frac{1}{2\rho^2} \left(\sum_{i=0}^{3} \xi_i^2 + \sum_{i=0}^{3} \psi_i^2 \cos^2\alpha \right) \right) \right. \\ & + \left. \frac{1}{2}\exp\left(-\frac{2}{3\rho^2} \left(\sum_{i=0}^{3} \xi_i^2 + \sum_{i=0}^{3} \psi_i^2 \cos^2\alpha \right) \right) \right] \cdot 2\xi_0 \exp(-\xi_0^2) d\xi_0 \ldots 2\xi_3 \exp(-\xi_3^2) d\xi_3 \\ & \cdot 2\psi_0 \exp(-\psi_0^2) d\psi_0 \ldots 2\psi_3 \exp(-\psi_3^2) d\psi_3. \end{aligned} \tag{II.6}$$

Since the vectors $\boldsymbol{h}_0$ and $\boldsymbol{h}_1$ are i.i.d. circularly symmetric complex normal vectors, it follows that α is statistically independent of ξ and ψ. From Eq. II.6 we get

$$\Pr\{\text{error}|\alpha\} \approx \frac{1}{6}\left(1+\frac{\overline{\gamma}}{2}\right)^{-4}\left(1+\frac{\overline{\gamma}\cos^2\alpha}{2}\right)^{-4}+\frac{1}{2}\left(1+\frac{2\overline{\gamma}}{3}\right)^{-4}\left(1+\frac{2\overline{\gamma}\cos^2\alpha}{3}\right)^{-4} \quad \text{(II.7)}$$

where $\overline{\gamma}=\rho^{-2}$. The error probability is found by integrating Eq. II.7 over all possible values of α, which requires knowledge of the probability density function (pdf) of α. The pdf of α for complex valued vectors of length n is given in [13]. In our case, when $n=4$, the pdf is given by $f_\alpha(\alpha)=6\sin^5\alpha\cos\alpha$, which yields the unconditional error probability

$$\begin{aligned}\Pr\{\text{error}\} \approx & \left(2\left(\frac{\overline{\gamma}}{2}\right)^2-\overline{\gamma}+2\right)\left(12\left(\frac{\overline{\gamma}}{2}\right)^3\left(1+\frac{\overline{\gamma}}{2}\right)^4\right)^{-1}\\ - & \left(4\left(\frac{\overline{\gamma}}{2}\right)^2+4\overline{\gamma}+4\right)\left(3\left(\frac{\overline{\gamma}}{2}\right)^3\left(1+\frac{\overline{\gamma}}{2}\right)^4(2+\overline{\gamma})^3\right)^{-1}\\ + & \left(\left(\frac{2\overline{\gamma}}{3}\right)^2-\frac{2\overline{\gamma}}{3}+1\right)\left(2\left(\frac{2\overline{\gamma}}{3}\right)^3\left(1+\frac{2\overline{\gamma}}{3}\right)^4\right)^{-1}\\ - & \left(4\left(\frac{2\overline{\gamma}}{3}\right)^2+\frac{16\overline{\gamma}}{3}+4\right)\left(\left(\frac{2\overline{\gamma}}{3}\right)^3\left(1+\frac{2\overline{\gamma}}{3}\right)^4\left(2+\frac{4\overline{\gamma}}{3}\right)^3\right)^{-1}. \quad \text{(II.8)}\end{aligned}$$

According to Eq. (II.8), the diversity order, defined as $\lim_{\overline{\gamma}\to\infty}\dfrac{-\log_e\Pr\{\text{error}\}}{\log_e\overline{\gamma}}$, is 5. The array gain, defined as the expected value of the post processing SNR given in Eq. (II.3) over the preprocessing SNR $=\overline{\gamma}$, is 7.09dB. Comparison between the error rate obtained by simulating this 4×2 MRT scheme and the theoretical error rate given by Eq. II.8, is shown in Fig. A.2. As seen, the theoretical and the simulated performance plots in Fig. A.2 coincide.

B. SM-MRT

Spatial Multiplexing (SM) is a scheme where multiple streams are transmitted concurrently. In the SM-MRT scheme considered here two data streams are transmitted concurrently, each from a different pair of antennas. In other words, two BS antennas transmit one stream and the other two transmit the second stream. As in the previous schemes, $\boldsymbol{h}_0$ is known to the BS while $\boldsymbol{h}_1$ is unknown. Define $\boldsymbol{h}_{0a}^*=[h_{00},h_{01}]$, $\boldsymbol{h}_{0b}^*=[h_{02},h_{03}]$, $\boldsymbol{h}_{1a}^*=[h_{10},h_{11}]$ and $\boldsymbol{h}_{1b}^*=[h_{12},h_{13}]$ so that $\boldsymbol{h}_0^*=[\boldsymbol{h}_{0a}^*,\boldsymbol{h}_{0b}^*]$ and $\boldsymbol{h}_1^*=[\boldsymbol{h}_{1a}^*,\boldsymbol{h}_{1b}^*]$.

The transmitted symbol vector is $\frac{1}{\sqrt{2}}\boldsymbol{s}$ where $\boldsymbol{s} = [s_0 \; s_1]^T$ is a vector of two independent QPSK symbols. The factor $\frac{1}{\sqrt{2}}$ is introduced in order to maintain unit transmission power. The precoding matrix $\boldsymbol{W}$ is given by

$$\boldsymbol{W} = \begin{bmatrix} \frac{h_{00}}{\|\boldsymbol{h}_{0a}\|} & \frac{h_{01}}{\|\boldsymbol{h}_{0a}\|} & 0 & 0 \\ & & & \\ 0 & 0 & \frac{h_{02}}{\|\boldsymbol{h}_{0b}\|} & \frac{h_{03}}{\|\boldsymbol{h}_{0b}\|} \end{bmatrix}, \tag{II.9}$$

and the received vector is

$$\boldsymbol{r} \;=\; \frac{1}{\sqrt{2}}\boldsymbol{H}\boldsymbol{W}^*\boldsymbol{s} + \rho\,\boldsymbol{n} = \frac{1}{\sqrt{2}} \underbrace{\begin{bmatrix} \|\boldsymbol{h}_{0a}\| & \|\boldsymbol{h}_{0b}\| \\ & \\ \|\boldsymbol{h}_{1a}\| z_1 \exp(j\theta) & \|\boldsymbol{h}_{1b}\| z_2 \exp(j\beta) \end{bmatrix}}_{\tilde{\boldsymbol{H}}} \boldsymbol{s} + \rho\,\boldsymbol{n} \tag{II.10}$$

where $\tilde{\boldsymbol{H}}$ is the equivalent channel matrix seen by the receiver, θ is the angle of the complex valued inner product of $\boldsymbol{h}_{0a}$ and $\boldsymbol{h}_{1a}$, β is the angle of the complex valued inner product of $\boldsymbol{h}_{0b}$ and $\boldsymbol{h}_{1b}$, z_1 and z_2 correspond to the cosine of the angle between the vectors similar to that defined in Eq. (II.5), and are distributed with $p(z_1) = 2z_1$ and $p(z_2) = 2z_2$ on $[0, 1]$. The angles θ and β are independent and uniformly distributed on $[0, 2\pi]$ [14].

In order to gain some intuition, we inspect the special form of the equivalent channel matrix $\tilde{\boldsymbol{H}}$, and assume for simplicity that the absolute value of each entry of $\tilde{\boldsymbol{H}}$ is in the vicinity of its expected value. In this case the matrix tends to be singular when $\theta \approx \beta$. The dominant error vector here is obviously an opposite sign error vector which brings the norm $\|\tilde{\boldsymbol{H}}\boldsymbol{e}\|$ close to zero.

An upper (union) bound for spatial multiplexing error probability is given by [15]

$$\Pr\left\{\text{error}|\tilde{\boldsymbol{H}}\right\} \leq \sum_{\boldsymbol{e}\in\,\mathscr{B}} Q\left((2\rho)^{-1}\|\tilde{\boldsymbol{H}}\boldsymbol{e}\|\right) \tag{II.11}$$

where $\boldsymbol{e}$ is an error vector and $\mathscr{B}$ is the set of all possible error vectors. Averaging with respect to the joint density function of $\tilde{\boldsymbol{H}}$ gives

$$\Pr\{\text{error}\} \leq \sum_{\boldsymbol{e}\in\,\mathscr{B}} \mathrm{E}\left\{Q\left((2\rho)^{-1}\|\tilde{\boldsymbol{H}}\boldsymbol{e}\|\right)\right\} \tag{II.12}$$

In classical open loop spatial multiplexing schemes, error vectors including one or two non-zero entries have similar likelihoods. In contrast to such classical schemes, in SM-MRT an error vector of type $\boldsymbol{e} = a[\sqrt{2}, -\sqrt{2}]^T$ where $a \in \{\pm 1, \pm j\}$ is more likely than all other error vectors. This phenomenon is demonstrated in this section by showing that the diversity order generated by the contribution of all other error vector types is significantly higher than the diversity order generated by the contribution of this error vector. The first step of this analysis is to evaluate the error probability of each error vector type. This is concluded by comparing between the error probabilities to show the dominance of the opposite sign error vector which are of type $\boldsymbol{e} = \begin{bmatrix} a & -a \end{bmatrix}^T$. For simplicity, we define $\boldsymbol{e}_1 = a\begin{bmatrix} \sqrt{2} & 0 \end{bmatrix}^T$, $\boldsymbol{e}_2 = a\begin{bmatrix} \sqrt{2} & \sqrt{2} \end{bmatrix}^T$ and $\boldsymbol{e}_3 = a\begin{bmatrix} \sqrt{2} & -\sqrt{2} \end{bmatrix}^T$ where $a \in \{\pm 1, \pm j\}$. Now we estimate the error probability of each error vector type.

1) Error probability for an error vector of type $\boldsymbol{e}_1$: The error probability of the single error vector $\boldsymbol{e}_1$, which is similar to the single error probability of the open loop spatial multiplexing, is

$$\Pr\{\text{error of type } \boldsymbol{e}_1\} \approx \frac{1}{6}\left(1+\frac{\overline{\gamma}}{8}\right)^{-3} + \frac{1}{2}\left(1+\frac{\overline{\gamma}}{6}\right)^{-3}. \tag{II.13}$$

Thus, the diversity order generated by a single error vector of type $\boldsymbol{e}_1$ is 3.

2) Error probability for an error vector of type $\boldsymbol{e}_2$: The error probability for the same sign error vector $\boldsymbol{e}_2$ is upper bounded by a bound similar to the error probability of the open loop spatial multiplexing scheme. Since the rows of $\tilde{\boldsymbol{H}}$ in Eq. (II.10) are independent, it suffices to look at the first row only in order to derive the bound. By approximating the Q-Function using an exponent for an error vector with the same sign entries, the conditional error probability becomes

$$\begin{aligned} \Pr\{\text{error of type } \boldsymbol{e}_2\} \approx & \int \left[\frac{1}{12}\exp\left(-(8\rho^2)^{-1}(\|\boldsymbol{h}_{0a}\| + \|\boldsymbol{h}_{0b}\|)^2\right)\right. \\ & + \left.\frac{1}{4}\exp\left(-(6\rho^2)^{-1}(\|\boldsymbol{h}_{0a}\| + \|\boldsymbol{h}_{0b}\|)^2\right)\right] \\ & \cdot \; p(\|\boldsymbol{h}_{0a}\|)p(\|\boldsymbol{h}_{0b}\|)d(\|\boldsymbol{h}_{0a}\|)d(\|\boldsymbol{h}_{0b}\|). \end{aligned} \tag{II.14}$$

The r.h.s. of Eq. (II.14) is bounded by

$$\begin{aligned} & \int \left[\frac{1}{12} \exp\left(-(8\rho^2)^{-1}(\|\boldsymbol{h}_{0a}\|^2 + \|\boldsymbol{h}_{0b}\|^2)\right) \right. \\ + \quad & \left. \frac{1}{4} \exp\left(-(6\rho^2)^{-1}(\|\boldsymbol{h}_{0a}\|^2 + \|\boldsymbol{h}_{0b}\|^2)\right) \right] \\ \cdot \quad & p(\|\boldsymbol{h}_{0a}\|)p(\|\boldsymbol{h}_{0b}\|)d(\|\boldsymbol{h}_{0a}\|)d(\|\boldsymbol{h}_{0b}\|) \\ = \quad & \frac{1}{6}\left(1+\frac{\overline{\gamma}}{8}\right)^{-4} + \frac{1}{2}\left(1+\frac{\overline{\gamma}}{6}\right)^{-4}, \end{aligned} \tag{II.15}$$

which implies that the error probability for an error of type $\boldsymbol{e}_2$ generates a diversity order of at least 4.

3) Error probability for an error vector of type $\boldsymbol{e}_3$: Inserting an error vector of type $\boldsymbol{e}_3$ into Eq. (II.11) results in

$$\Pr\left\{\text{error of type } \boldsymbol{e}_3 | \tilde{\boldsymbol{H}}\right\} = Q\left((2\rho)^{-1}\|\tilde{\boldsymbol{H}} a \begin{bmatrix} \sqrt{2} & -\sqrt{2} \end{bmatrix}^T \|\right),\ a \in \{\pm 1, \pm j\}. \tag{II.16}$$

Unlike the case in Eq. (II.15) of an error vector of type $\boldsymbol{e}_2$ where the integral's bound was easily found, this case is more complicated. The error probability for this scheme is approximated by (see Appendix A)

$$\Pr\{\text{error of type } \boldsymbol{e}_3\} \approx 9\pi^{-7}2^{-10}\overline{\gamma}^{10}(1+\overline{\gamma})^{-6.5}(1+0.0062\overline{\gamma}^2)^{-2.5}, \tag{II.17}$$

which implies a diversity order of 1.5 generated by an error vector of type $\boldsymbol{e}_3$.

4) Comparison between error vector types: Comparing the error probability associated with each error vector type, the diversity order of an error vector of type $\boldsymbol{e}_3$ is the smallest, hence error of type $\boldsymbol{e}_3$ is most dominant at high SNR. Therefore, we can write the error probability for this scheme as

$$\begin{aligned} \Pr\{\text{error}\} & \approx \Pr\{\text{error of type } \boldsymbol{e}_3\} \\ & \approx 9\pi^{-7}2^{-10}\overline{\gamma}^{10}(1+\overline{\gamma})^{-6.5}(1+0.0062\overline{\gamma}^2)^{-2.5}. \end{aligned} \tag{II.18}$$

The diversity order, which was derived from Eq. (II.18), is 1.5. In order to evaluate the scheme's array gain, we use the fact that when the error rate of a spatial multiplexing scheme is given by

$$\Pr\{\text{error}\} = \left(1+\frac{\overline{\gamma}}{2M}\right)^{-N}, \tag{II.19}$$

then the array gain is $\frac{N}{M}$. We ignore non dominant terms in the high SNR regime to rewrite Eq. (II.18) in the form of Eq. (II.19). The resulting array gain is 4.97dB. The dominance of the error vector of type $\boldsymbol{e}_3$ in high SNR regime, as observed in simulations, is seen in Fig. A.3.

Simulation results for the SM-MRT scheme that uses Eq. (II.18) and its comparison to theoretical results are given in Fig. A.4. As we see, theoretical and practical performance plots are overlaid in the high SNR regime.

III. Simulation Results

The optimal solution in the SNR sense when full channel knowledge is available at the transmitter is the well known eigenbeamforming scheme [16]. The diversity order of this scheme with M transmit antennas and N receive antennas is MN and the array gain is bounded by MN and $\max(M, N)$ [17]. Specifically, when $M = 4$ and $N = 2$, the array gain is analytically calculated as 7.91dB. A comparison between the performances of the two analyzed techniques and the optimal eigenbeamforming technique in uncorrelated Rayleigh fading channels is given in Fig. A.6. We see that the 4×2 Eigen Beamformer provides a higher diversity order and higher array gain than what the other schemes achieve. Although the 4×2 MRT scheme has a higher diversity order than what the SM-MRT scheme achieves, we keep in mind that the SM-MRT scheme provides double throughput when compared to the 4×2 MRT scheme. In order to compare between the schemes with the same throughput, the simulations were repeated for twice the bit rate of single stream schemes that use 16QAM modulation. Results are given in Fig. A.5. As expected, the results for both single stream schemes were shifted to the right by approximately 6-7 dB, while maintaining identical diversity order.

The performance of the suboptimal 4×2 MRT scheme is close to the optimal scheme especially at low SER values. For example, the performance degradation of the suboptimal 4×2 MRT scheme at SER $= 10^{-6}$ is approximately 4dB. This scheme has relatively high array gain and high diversity order.

After the analysis and simulation of the suboptimal schemes in classical uncoded Rayleigh fading channels were completed, we now analyze the performance of these schemes in benchmark WiMAX channels. These results will provide us with an insight into the performance in real situations. It will also corroborate the results obtained earlier by showing similar characteristics.

Several channel models were defined by the International Telecommunications Union (ITU) [18]. Each assumes a different number of taps, delays, powers and Doppler spectrum. One of the most popular channel models, which was used within the WiMAX community as a benchmark to validate results, is the Pedestrian B channel model. We compare between the results of the three schemes in the Pedestrian B channel when all the channels are uncorrelated and forward error correction is not used. Then, we compare between them utilizing error correction. In order to be consistent with the flat fading case, orthogonal frequency division multiplexing (OFDM) modulation was employed and sufficiently long guard interval was assumed. For simplicity, results derived from the use of the encoder are shown in terms of bit error rate and not by symbol error rate. Results for the uncoded case are given in Fig. A.7. The results are similar to those from uncorrelated Rayleigh fading channel as was presented in Fig. A.5. We simulate now the three schemes in uncorrelated Pedestrian B channels when error correction is employed. The convolutional Turbo Code (CTC) encoder, as defined in the 802.16 standard [19], is used in these simulations. Initially, a low rate coding scheme at low SNR values is used. Then, we compare between the three schemes when we assign high modulations and high coding rates to the schemes, while maintaining equal throughput among the schemes.

Fig. A.8 shows that by using error correction with low coding rate, the schemes function well in very low SNR. However, the qualitative relationship between the schemes still holds. The suboptimal 4×2 MRT scheme performs similarly to the optimal scheme, whereas there is still a large gap compared to the suboptimal SM-MRT scheme.

Fig. A.9 shows a comparison between the performance of these schemes that have high throughput and high coding rates. In this case of high coding rate, the gaps between them are small when the schemes operate at high SNR values. The suboptimal SM-MRT scheme is approximately 1dB worse than the suboptimal 4×2 MRT scheme at BER=10^{-4}. It is expected that as the SNR becomes high, the performance of high throughput spatial multiplexing schemes becomes better. This is shown for example in [11]. However, since the WiMAX standard does not support modulation higher than 64QAM, it is impossible to compare between equal throughput schemes at a high SNR range. At high SNR values, where single stream schemes are capped at throughput, it is advantageous to employ the suboptimal SM-MRT scheme. In addition, if modulations higher than 64QAM were supported, it is expected that SM-MRT outperforms the other schemes at high SNR values.

The analysis and the simulations in this paper were based on averaging of all channel realizations (without any selection mechanism). There may be occasions where a specific channel realization will enable the suboptimal SM-MRT scheme to outperform other schemes. Since mode selection modules in practical systems (specifically those optimized for low mobility) often select the mode that is optimal for the measured channel realization at hand (and not according to the statistics of the channel), it is possible to employ the SM-MRT scheme for such channel realizations.

IV. CONCLUSIONS

In this paper, we analyzed the performance of suboptimal MIMO schemes which are common in WiMAX and in LTE systems. The optimal eigen-beamforming scheme acted as a reference for performance comparisons of the sub-optimal schcmes in terms of error probability, diversity order and array gain. The results from these comparisons are surprising - the array gain of the 4×2 MRT scheme is similar to the array gain of the optimal scheme. Although the diversity order of this sub-optimal scheme is lower than the high diversity order of the optimal scheme (5 and 8, respectively), it is still significantly high, while resulting in low error rates.

The SM-MRT scheme, on the other hand, displays far worse results. Its diversity order (1.5) is even lower than 2×2 open loop spatial multiplexing (for which the diversity order is 2). Thus, in high SNR values it is better to use open loop spatial multiplexing than to use the SM-MRT scheme. Even in coded systems, the SM-MRT scheme performs worse than the 4×2 MRT scheme, although the gap between these two schemes becomes low as the SNR increases. The array gain of the SM-MRT scheme is also lower than the array gain of the optimal and the 4×2 MRT schemes.

The optimal scheme for a specific MIMO scenario discussed here requires the MS to transmit using two antennas, which increases the cost and the complexity of an MS. Furthermore, the optimal scheme requires a singular value decomposition (SVD) calculation at the transmitter, which adds to the complexity of the implementation. The performance analysis and the comparisons in this paper show that low complexity sub-optimal schemes, such as the 4×2 MRT scheme, can replace high complexity optimal schemes without causing a major performance degradation.

APPENDIX A
EVALUATION OF THE ERROR PROBABILITY FOR AN ERROR VECTOR OF TYPE e_3

In this appendix, we calculate the expectation of Eq. (II.16) w.r.t. $\tilde{\boldsymbol{H}}$. We begin by giving an overview of the solution, followed by calculating the kernel integral which corresponds to the first row of $\tilde{\boldsymbol{H}}$. We then extend this solution to the second row of $\tilde{\boldsymbol{H}}$, and combine both to get the overall error probability.

1) Overview of the solution for error probability of type $\boldsymbol{e}_3$: Before we evaluate the bound in Eq. (II.16), we examine the structure of $\tilde{\boldsymbol{H}}$ defined in Eq. (II.10). After the multiplication of the first row of $\tilde{\boldsymbol{H}}$ by the error vector $\boldsymbol{e}_3$, the numerator within the exponent, which approximates the Q-Function, is

$$|\tilde{\boldsymbol{h}}^{(1)}\boldsymbol{e}_3|^2 \;=\; 2\left[\|\boldsymbol{h}_{0a}\|^2+\|\boldsymbol{h}_{0b}\|^2-2\|\boldsymbol{h}_{0a}\|\|\boldsymbol{h}_{0b}\|\right], \tag{A.1}$$

where $\tilde{\boldsymbol{h}}^{(i)}$ corresponds to the i-th row of $\tilde{\boldsymbol{H}}$. Similarly, after the multiplication of the second row of $\tilde{\boldsymbol{H}}$ by the error vector $\boldsymbol{e}_3$, the numerator within the exponent becomes

$$\begin{aligned}|\tilde{\boldsymbol{h}}^{(2)}\boldsymbol{e}_3|^2 &= \left|\begin{bmatrix}\|\boldsymbol{h}_{1a}\|z_1\exp(j\theta) & \|\boldsymbol{h}_{1b}\|z_2\exp(j\beta)\end{bmatrix}\boldsymbol{e}_3\right|^2\\ &= 2\left[\|\boldsymbol{h}_{1a}\|^2z_1^2+\|\boldsymbol{h}_{1b}\|^2z_2^2-2\|\boldsymbol{h}_{1a}\|\|\boldsymbol{h}_{1b}\|z_1z_2\cos(\delta)\right],\ \delta=\theta-\beta.\end{aligned} \tag{A.2}$$

Since θ and β are uniformly and independently distributed on $[0,2\pi]$, $p(\delta)=\dfrac{(2\pi-|\delta|)}{4\pi^2}$ on $[-2\pi,2\pi]$. Thus, the result for the second row of $\tilde{\boldsymbol{H}}$ is an extension (via the angle δ) of the contribution of the first row of $\tilde{\boldsymbol{H}}$. In other words, since the rows of $\tilde{\boldsymbol{H}}$ are independent, we can integrate Eq. (II.16) on the contribution of the first row of $\tilde{\boldsymbol{H}}$ and then reuse it for the second row by integrating over the angle δ. The kernel integral to be solved, which corresponds to the first row of $\tilde{\boldsymbol{H}}$, becomes

$$\Pr\{\text{error of type }\boldsymbol{e}_3\}=\iint\limits_{\boldsymbol{a},\boldsymbol{b}\in\mathbb{C}^2}\exp\left((-2\rho^2)^{-1}(\|\boldsymbol{a}\|-\|\boldsymbol{b}\|)^2\right)p(\boldsymbol{a})p(\boldsymbol{b})d\boldsymbol{a}d\boldsymbol{b}\triangleq I_1, \tag{A.3}$$

where $\boldsymbol{a}$ and $\boldsymbol{b}$ are complex Gaussian vectors of length 2.

2) Evaluation of the kernel integral: The kernel integral I_1, defined in Eq. (A.3), is solved for both rows of $\tilde{\boldsymbol{H}}$. Since both rows are independent, we solve for the first row and afterwards this solution is extended to the second row. Consider the kernel integral in Eq. (A.3), where $\boldsymbol{a}=(x_1+iy_1,x_2+iy_2),\boldsymbol{b}=(u_1+iv_1,u_2+iv_2)$, and

$$p(\boldsymbol{a})\triangleq(2\pi\sigma^2)^{-2}\exp\left(-(2\sigma^2)^{-1}(x_1^2+y_1^2+x_2^2+y_2^2)\right),\ \sigma^2=\frac{1}{2}. \tag{A.4}$$

By changing the integral in Eq. (A.3) to spherical coordinates in $\mathbb{R}^4$, we get

$$I_1(\alpha,\eta) = (\eta^2-\alpha)^4\pi^{-4}\int_0^\infty\int_0^\infty x^3\exp\left(2\alpha xy-\eta^2x^2\right)y^3\exp\left(-\eta^2y^2\right)dxdy, \qquad \text{(A.5)}$$

where $\alpha=(2\rho^2)^{-1}$, and $\eta^2=(2\sigma^2)^{-1}+\alpha$. The variables x and y are the radial variables in spherical representation. The result of the integral in Eq. (A.5) is

$$\begin{aligned} I_1(\alpha,\eta) &= 25\pi^{-4}\left[2(\eta^4-\alpha^2)^4\right]^{-1}\left[-22\alpha^4+12\alpha^3\arctan\left(\frac{\alpha}{\sqrt{\eta^4-\alpha^2}}\right)\sqrt{\eta^4-\alpha^2}\right. \\ &+ 6\alpha^3\pi\sqrt{\eta^4-\alpha^2}+14\alpha^2\eta^4+9\alpha\pi\sqrt{\eta^4-\alpha^2}\eta^4 \\ &+ \left.18\alpha\eta^4\sqrt{\eta^4-\alpha^2}\arctan\left(\frac{\alpha}{\sqrt{\eta^4-\alpha^2}}\right)+8\eta^8\right]. \qquad \text{(A.6)} \end{aligned}$$

At high SNR values, which form the regime we are most interested in, the values of α and η^2 are almost identical, and the integral can be approximated by

$$I_1(\alpha) \approx 375\pi^{-3}\alpha^3(1+2\alpha)^{-3.5} = 375\left(\overline{\gamma}/2\pi\right)^3(1+\overline{\gamma})^{-3.5}, \qquad \text{(A.7)}$$

implying a diversity order of $\frac{1}{2}$ generated by the first row of $\tilde{\boldsymbol{H}}$.

3) Extension to the second row of $\tilde{\boldsymbol{H}}$: Incorporating the second row of $\tilde{\boldsymbol{H}}$ given by Eq. (A.2), we extend the kernel integral to give

$$\begin{aligned} I_2(\alpha,\eta) &= \int_{x=0}^{\infty}\int_{y=0}^{\infty}\int_{z_1=0}^{1}\int_{z_2=0}^{1}\int_{\delta=-2\pi}^{2\pi}\exp\left\{-\frac{x^2z_1^2+y^2z_2^2-2xyz_1z_2\cos(\delta)}{2\rho^2}\right\} \\ &\cdot \pi^{-4}x^3y^3\exp\left\{-(x^2+y^2)\right\}2z_1 2z_2\frac{(2\pi-|\delta|)}{4\pi^2}dx\,dy\,dz_1\,dz_2\,d\delta. \qquad \text{(A.8)} \end{aligned}$$

We begin by analyzing the impact of the angle δ on the integrand, by numerically integrating for fixed values of δ. As can be seen in Fig. A.10, the integrand's contribution is most dominant when δ approaches zero.

We continue by looking at the impact of z_1 and z_2 on the integrand for a fixed δ, numerically integrating over all values of x and y. The value of the integrand as a function of z_1 and z_2 when $\delta=0$ and SNR =30dB is shown in Fig. A.11. As can be seen, the integrand's contribution is most dominant when z_1 and z_2 approach one. Intuitively, this point is dominant because the resulting equivalent channel matrix $\tilde{\boldsymbol{H}}$ is made up of same sign entries in the second row, resulting from $\delta=0$, and gain that tends to be similar, resulting from $z_1=z_2=1$. Such a structure tends to decrease the condition number, increasing the

error probability. We compare these results with the value of the integral when $\delta = 0.1\pi$, as shown in Fig. A.12. As can be seen, for a slightly increased δ, the main contribution of the integrand is now centered around z_1 and z_2 much closer to zero. However, the integrand's value is orders of magnitude smaller. This phenomenon is more pronounced as δ is increased.

We may thus focus on z_1, $z_2 \longrightarrow 1$ in order to compute the integral in Eq. (A.8), rewriting it in the following form,

$$\begin{aligned} I_2(\alpha,\eta) &= \pi^{-6} \int_0^{\infty}\int_0^{\infty}\int_{\delta=-2\pi}^{2\pi} x^3 y^3 \exp\left\{-\frac{x^2+y^2-2xy\cos\delta}{2\rho^2}\right\} \exp\left\{-(x^2+y^2)\right\} \\ &\cdot (2\pi - |\delta|) dx dy d\delta, \end{aligned} \tag{A.9}$$

which is an upper bound on the error probability since the maximum value of z_1 and z_2 was incorporated. The result of this integral, given δ, may be derived by extending the kernel integral in Eq. (A.7), replacing α in Eq. (A.6) by $\tilde{\alpha} = \alpha\cos(\delta)$ where η^2 is not modified. At high SNR values, where $\eta^2 \approx \alpha$, and looking at the dominant terms, the integral over δ becomes

$$\begin{aligned} I_2(\alpha) &\approx 150\alpha^3\pi^{-6} \int_{-2\pi}^{2\pi} (2\pi - |\delta|)(1+2\alpha+\alpha^2\sin\delta^2)^{-3.5}\cos\delta \\ &\cdot \arctan\left(\alpha(1-0.5\delta^2)(1+2\alpha+\alpha^2\delta^2)^{-0.5}\right)(2\cos\delta^2+3)d\delta. \end{aligned} \tag{A.10}$$

The integrand in Eq. (A.10) is Taylor expanded around $\delta = 0$. We use the approximations $\cos^2(\delta) \approx 1-\delta^2$, $\cos(\delta) \approx 1-0.5\delta^2$, $\sin^2(\delta) \approx \delta^2$ and $\arctan(x) \approx -18.02x^3 + 11.79x^2 - 3.37x + 1.499$, where the last approximation holds for $|\delta| < 0.05\pi$ (implying a large x) which is where the integrand is most dominant. Incorporating all approximations, the integral can be shown to be

$$I_2(\alpha) \approx 0.012\pi^{-4}\alpha^7(1+2\alpha)^{-3}(1+0.0247\alpha^2)^{-2.5}, \tag{A.11}$$

which implies a diversity order of 1 generated by the second row of $\tilde{\boldsymbol{H}}$.

4) Combined error probability for an error vector of type $\boldsymbol{e}_3$: This scheme's error probability, as defined in Eq. (II.16), consists of two independent components: a) One is derived from the first row of $\tilde{\boldsymbol{H}}$ and is given by Eq. (A.7). b) The second component is generated by the second row of $\tilde{\boldsymbol{H}}$ and is given by Eq. (A.11). Combination of the two components yields

the scheme's error probability. Since both rows of $\tilde{\boldsymbol{H}}$ are independent, we can multiply both results. We have to take into account the error vector's magnitude of two, thus, the scheme's combined error probability is given by

$$\begin{aligned}\Pr\{\text{error of type } \boldsymbol{e}_3\} &\approx 2I_1 I_2 \\ &= 9\pi^{-7}2^{-10}\overline{\gamma}^{10}(1+\overline{\gamma})^{-6.5}(1+0.0062\overline{\gamma}^2)^{-2.5}, \quad \text{(A.12)}\end{aligned}$$

which implies a diversity order of 1.5 generated by an error vector of type $\boldsymbol{e}_3$.

ACKNOWLEDGMENT

This research was supported by the Israel Science Foundation (grant No. 218/08), by the Institute for Future Technologies Research named for the Medvedi, Shwartzman and Gensler Families.

REFERENCES

[1] S. Alamouti, "A simple transmit diversity technique for wireless communications," *IEEE J. Sel. Areas Comm.*, vol. 16, no. 8, pp. 1451–1458, Oct 1998.

[2] D. J. Love and R. W. Heath, "Limited feedback unitary precoding for spatial multiplexing systems," *IEEE Trans. on Inform. Theory*, vol. 51, no. 8, pp. 2967–2976, Aug 2005.

[3] D. J. Love, R. W. Heath, W. Santipach, and M. L. Honig, "What is the value of limited feedback for mimo channels?" *IEEE Communications Magazine*, vol. 42, no. 10, pp. 54–59, Oct 2004.

[4] D. J. Love, S. Member, R. W. Heath, and T. Strohmer, "Grassmannian beamforming for multiple-input multiple-output wireless systems," *IEEE Trans. on Inform. Theory*, vol. 49, no. 10, pp. 2735–2747, Oct 2003.

[5] N. Jindal, "Mimo broadcast channels with finite rate feedback," *IEEE Trans. on Inform. Theory*, vol. 52, no. 11, pp. 5045–5060, Nov 2006.

[6] D. Gesbert, M. Kountouris, R. W. Heath, C. byoung Chae, and T. Saelzer, "From single user to multiuser communications: Shifting the mimo paradigm," *IEEE Sig. Proc. Magazine*, vol. 24, no. 5, pp. 36–46, Sep 2007.

[7] F. Kaltenberger, M. Kountouris, D. Gesbert, and R. Knopp, "Performance of multi-user mimo precoding with limited feedback over measured channels," in *Proc. IEEE Global Communications Conference (IEEE GLOBECOM 2008)*, New Orleans, USA, Nov-Dec 2008.

[8] S. Sesia, I. Toufik, and M. Baker, Eds., *LTE, The UMTS Long Term Evolution: From Theory to Practice*. Wiley, Feb 2009, ch. 17.

[9] "Wimax forum mobile system profile, release 1.0 approved specification, revision 1.61," 2008.

[10] R. W. Heath and A. J. Paulraj, "Switching between diversity and multiplexing in mimo systems," *IEEE Trans. on Comm.*, vol. 53, no. 2, pp. 962–968, Jun 2005.

[11] X. Zhuang, F. W. Vook, and T. A. Thomas, "Ofdm multi-antenna designs with concatenated codes," in *Global Telecommunications Conference (GLOBECOM)*, vol. 1, Nov. 2002, pp. 666–670.

[12] M. Chiani and D. Dardari, “Improved exponential bounds and approximations for the q-function with application to average error probability computation,” vol. 2. GLOBECOM, Nov 2002, pp. 1399–1402.

[13] S. Loyka and F. Gagnon, “Performance analysis of the v-blast algorithm: An analytical approach,” *IEEE Trans. on Wireless Comm.*, vol. 3, no. 4, pp. 1326–1337, Jul 2004.

[14] A. Abdi, H. Hashemi, and S. Nader-Esfahani, “On the pdf of the sum of random vectors,” *IEEE Trans. on Comm.*, vol. 48, no. 1, pp. 7–12, Jan 2000.

[15] V. Tarokh, N. Seshadri, and A. R. Calderbank, “Space time codes for high data rate wireless communication: Performance criterion and code construction,” *IEEE Trans. on Inform. Theory*, vol. 44, no. 2, pp. 744–765, Mar 1998.

[16] J. S. Hammerschmidt, C. Brunner, and C. Drewes, “Eigenbeamforming - a novel concept in array signal processing,” in *Proc. European Wireless*, Dresden, Germany, Sep 2000.

[17] A. Paulraj, R. Nabar, and D. Gore, *Introduction to Space-Time Wireless Communications*. New York, NY, USA: Cambridge University Press, 2008.

[18] “Recommendation ITU-R M.1225: Guidelines for Evaluation of Radio Transmission Technologies for IMT-2000, ITU,” 1997.

[19] “IEEE Std 802.16e. IEEE Standard for Local and Metropolitan Area Networks, Part 16: Air Interface for Fixed and Mobile Broadband Wireless Access Systems, IEEE,” 2005.

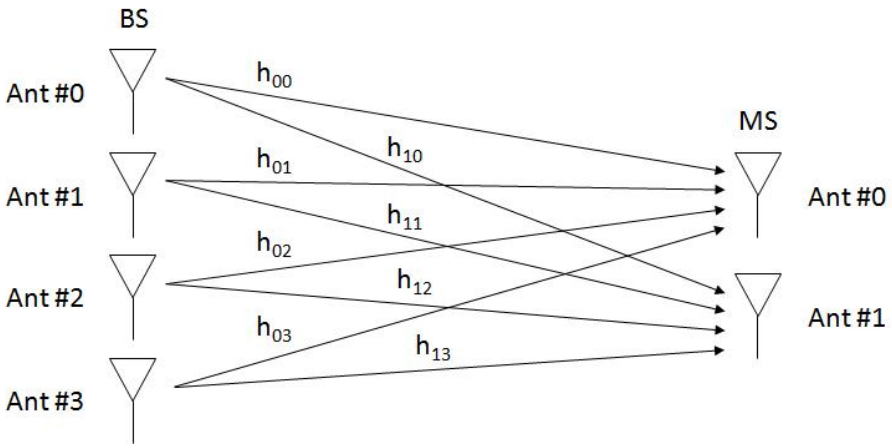

Fig. A.1. Basic 4 × 2 antenna scheme.

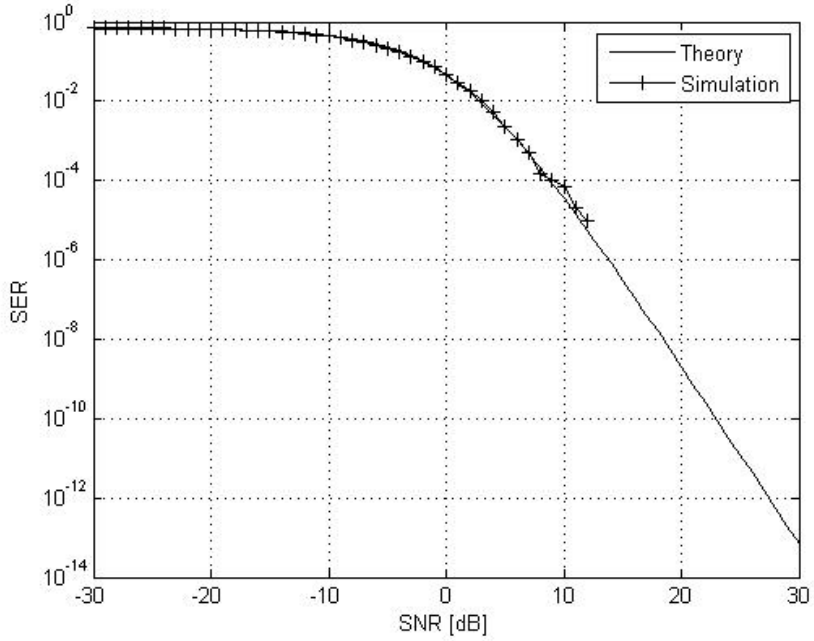

Fig. A.2. Performance comparison between theoretical and simulation results for the suboptimal 4×2 MRT scheme.

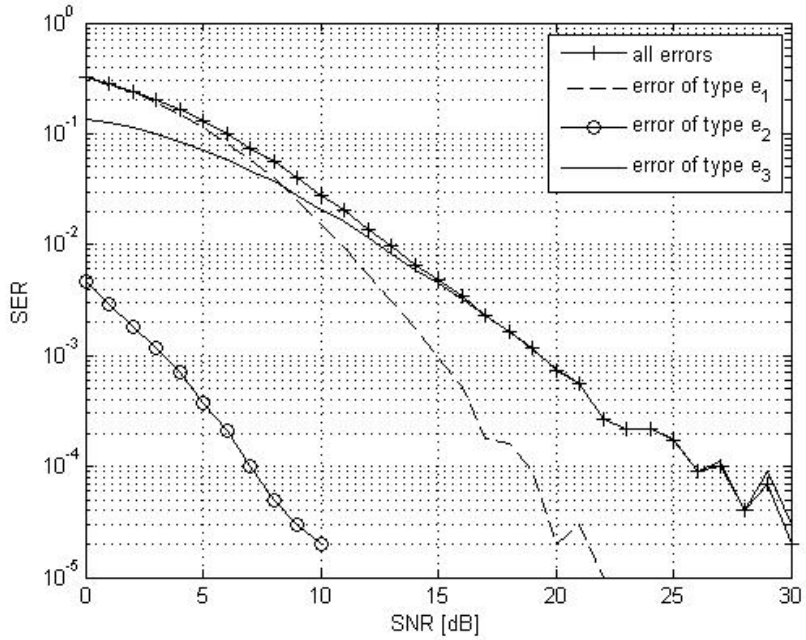

Fig. A.3. Comparison between the error probabilities of the SM-MRT scheme for all the errors and errors of types $\boldsymbol{e}_1$, $\boldsymbol{e}_2$ and $\boldsymbol{e}_3$, as observed in simulations.

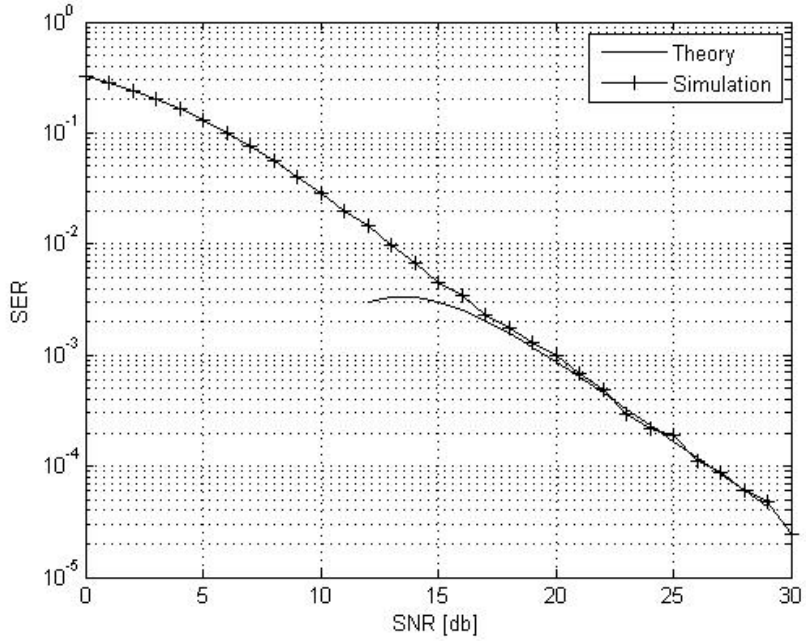

Fig. A.4. Performance comparison between theoretical and simulation results for the suboptimal SM-MRT scheme.

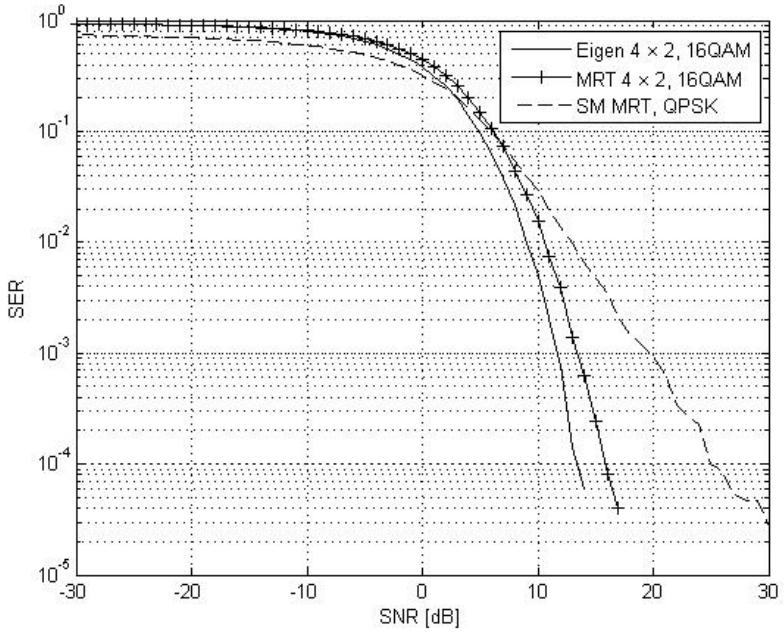

Fig. A.5. Performance comparison between all the three schemes in uncorrelated Rayleigh fading channels with equal throughput.

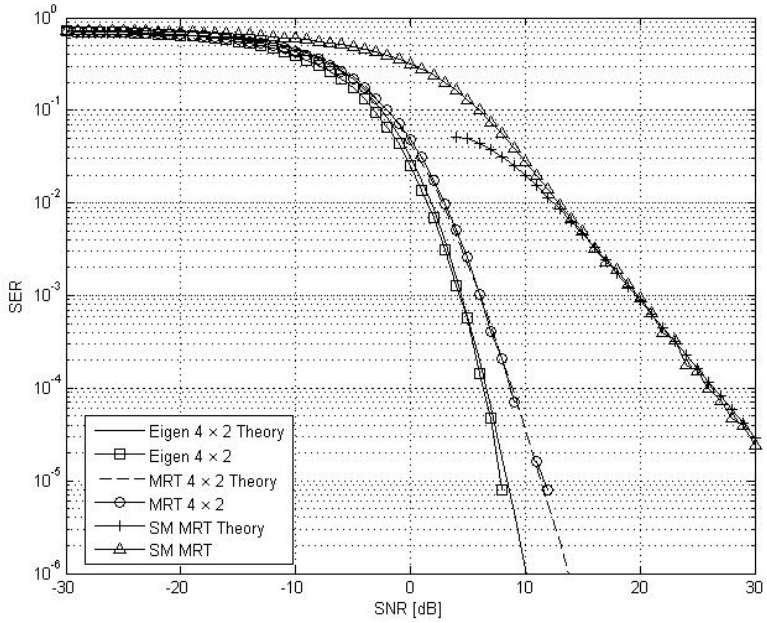

Fig. A.6. Performance comparison between all the three schemes in uncorrelated Rayleigh fading channels using QPSK modulation.

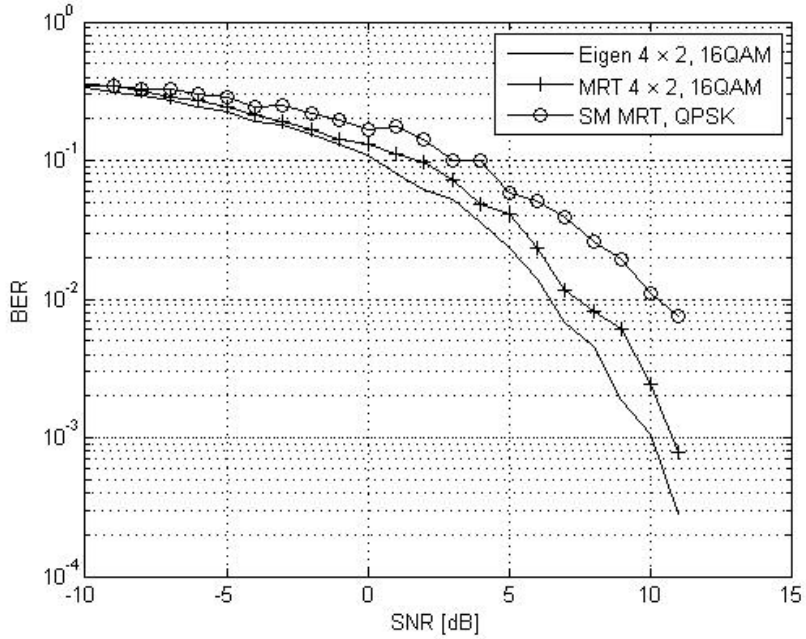

Fig. A.7. Performance comparison between the three schemes in uncorrelated Pedestrian B channels without error coding.

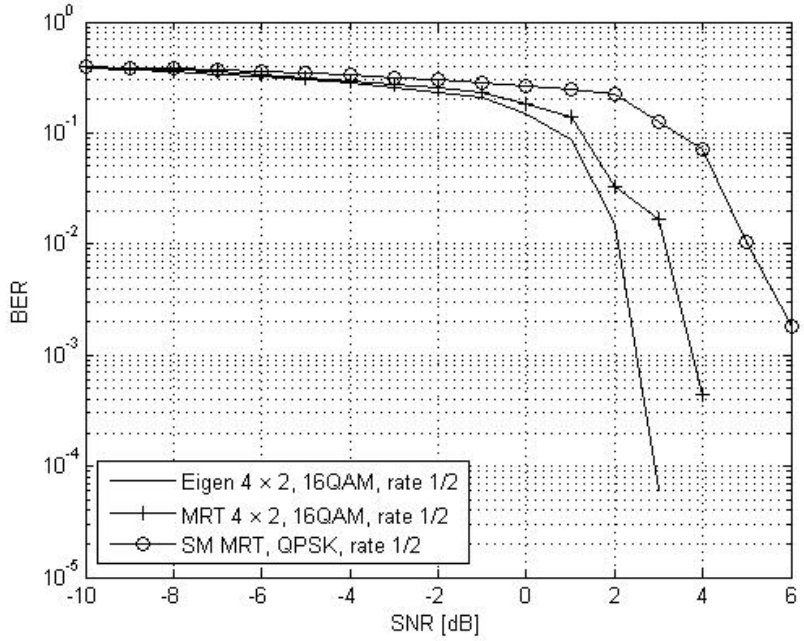

Fig. A.8. Performance comparison between the three schemes in uncorrelated Pedestrian B channels with low rate error coding while maintaining an equal throughput.

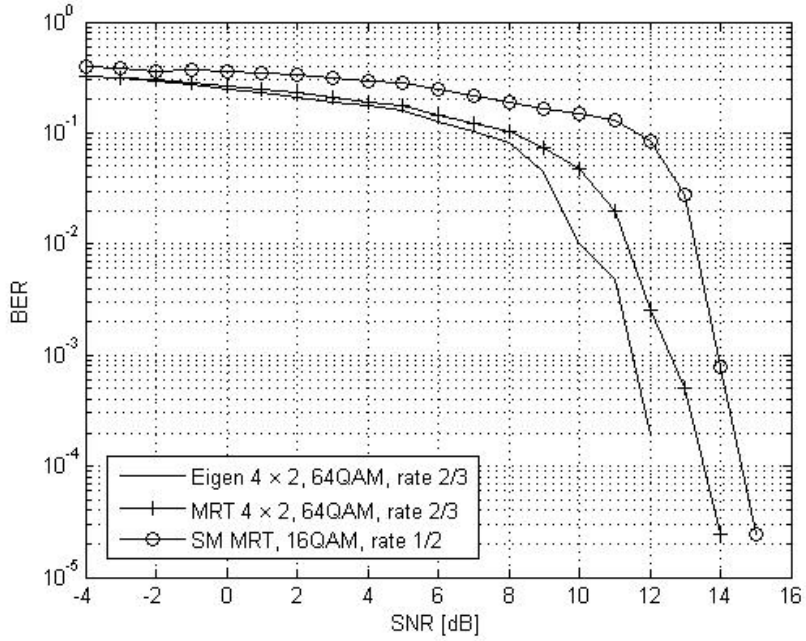

Fig. A.9. Performance comparison between the three schemes in uncorrelated Pedestrian B channels with high rate error coding while maintaining an equal throughput.

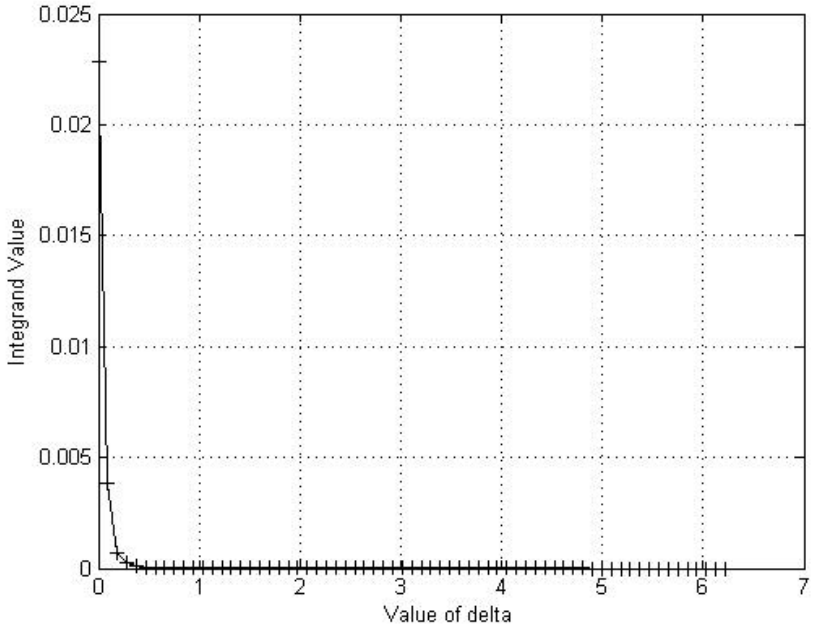

Fig. A.10. Value of the integrand in Eq. (A.8) as a function of δ.

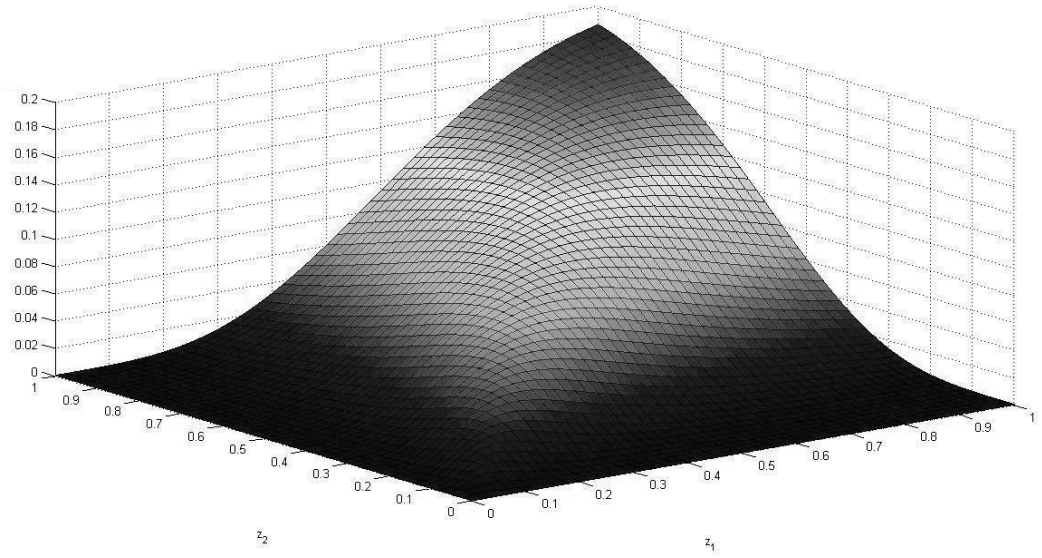

Fig. A.11. Value of the integrand in Eq. (A.8) as a function of z_1 and z_2 for SNR $= 30$dB and $\delta = 0$.

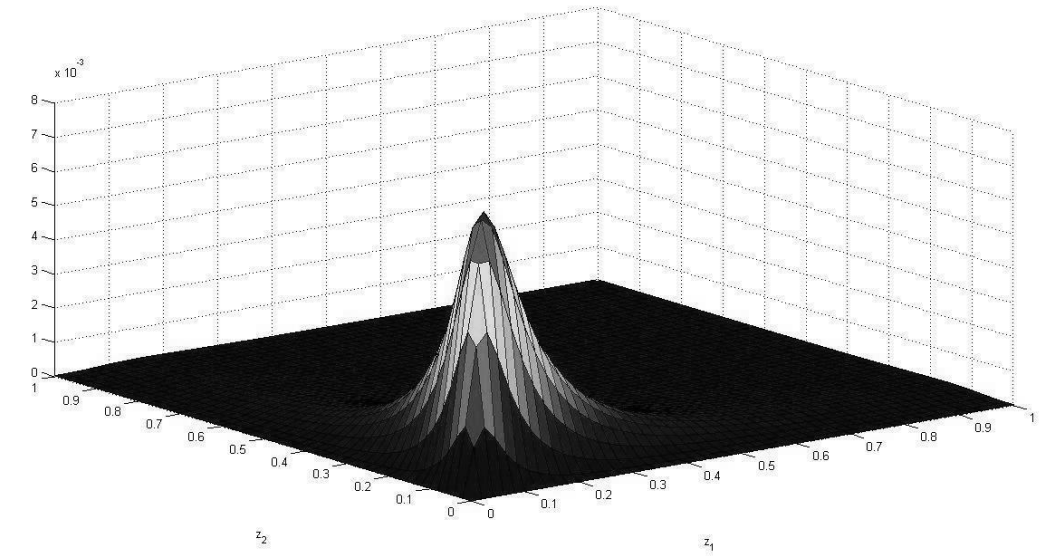

Fig. A.12. Value of the integrand in Eq. (A.8) as a function of z_1 and z_2 for SNR $= 30$dB and $\delta = 0.1\pi$.